A field study on ice melting and breakup in a boreal lake, Pääjärvi, in Finland

Yaodan Zhang[1,2], Marta Fregona[3], John Loehr[2], Joonatan Ala-Könni[4], Shuang Song[5,6], Matti Leppäranta[4], and Zhijun Li[1]

[1]State Key Laboratory of Coastal and Offshore Engineering, Dalian University of Technology, Dalian, China
[2]Lammi Biological Station, University of Helsinki, Finland
[3]Department of Civil, Environmental and Mechanical Engineering, University of Trento, Trento, Italy
[4]Institute of Atmospheric and Earth Sciences, University of Helsinki, Helsinki, Finland
[5]Water Conservancy and Civil Engineering College, Inner-Mongolia Agricultural University, Hohhot, China
[6]College of Water Conservancy, Shenyang Agricultural University, Shenyang, China

Correspondence to: Zhijun Li (lizhijun@dlut.edu.cn), Yaodan Zhang (zhangyaodan@mail.dlut.edu.cn).

Abstract. Lake ice melting and breakup form a fast, nonlinear process with important mechanical, chemical, and biological consequences. The process is difficult to study in the field due to safety issues, and therefore only little is known about its details. In the present work, the field data were collected on foot, by hydrocopter, and by boat for a full time-series of the evolution of ice thickness, structure, and geochemistry through the melting period. The observations were made in Lake Pääjärvi in 2018 (pilot study) and 2022. In 2022, the maximum thickness of ice was 55 cm with 60 % snow-ice, and in 40 days the ice melted by 33 cm from the surface and 22 cm from the bottom while the porosity increased from less than 5% to $40-50$ % at breakup. In 2018, the snow-ice layer was thin, and bottom and internal melting dominated the ice decay. The mean melting rates were 1.31 cm d^{-1} in 2022 and 1.55 cm d^{-1} in 2018. In 2022 the electrical conductivity (EC) of ice was 11.4 $\pm$ 5.79 μS cm^{-1}, one order of magnitude lower than in the lake water, and ice pH was 6.44 $\pm$ 0.28, lower by 0.4 than in water. The pH and EC of ice and water decreased along the ice decay except for slight increases in ice due to flushing by lake water. Chlorophyll *a* was less than 0.5 μg L^{-1} in porous ice, approximately one-third of that in the lake water. The results are important for understanding the process of ice decay with consequences to lake ecology, further development of numerical lake ice models, and modeling the safety of ice cover and ice loads.

1 Introduction

Lake ice is a thin layer between the atmosphere and lake water body and plays an important role in the local environment and human life (Leppäranta, 2015). Lake ice affects the local weather by altering the heat, mass and momentum exchange between the atmosphere and lake water body, as seen in the surface roughness, surface temperature and albedo (Ellis and Johnson, 2004; Rouse et al., 2008a, 2008b; Williams et al., 2004). The physical properties of an ice cover are determined by the stratification, crystal structure, and gas bubbles and other impurities. They control ice mechanics, growth and decay of ice, and transfer of sound and electromagnetic signals which have a key role in lake ice remote sensing, under-ice living conditions, and ice ecology (Iliescu and Baker, 2007; Li et al., 2010; Shoshany et al., 2002). Although most boreal lakes possess a seasonal ice cover, lake research has traditionally focused on summer, and especially little is known about the ice decay period when the ice melts, weakens, and disappears. The obvious reason is that fieldwork is then logistically very difficult. However, the structure and properties of ice undergo rapid changes during the decay period that has an important influence on the conditions in and below the ice cover.

There are two major practical problems with melting lake ice due to the loss of strength caused by the ice deterioration (Ashton, 1985; Leppäranta, 2015; Masterson, 2009). First, the bearing capacity of ice decreases, and therefore on-ice traffic becomes risky. Accidents are reported every spring due to the weak ice, connected with fishing or crossing of lakes. Second, a weakened ice cover may be broken, forced drifting by wind, and pushed onshore. Such ice with finite strength is a risk for structures near the shore, such as docks and bridges, and may cause near-shore erosion. Hence, it is urgent to study the physical properties of ice during the melting period.

The climatology of ice breakup date has been widely studied based on long-term time-series records (Benson et al., 2012; Korhonen, 2006; Karetnikov et al., 2017; Magnuson et al., 2000). A steady trend toward earlier melting date has been reported in most recent ice phenology studies, by about one week over 100 years in boreal lakes, attributed to the global climate warming. Numerical modelling studies of ice breakup have revealed that the time when ice starts to melt and internal melting of ice have major impacts on the accuracy of the simulations (Yang et al., 2012). The timing of ice breakup is

a question of atmospheric warming and falling albedo (Leppäranta, 2014), and its proper solution requires a quantification of the physical mechanisms that control the melting of ice.

The trend toward earlier breakup has been suggested as a driving factor to changes of ecological and biogeochemical processes in seasonally ice-covered lakes (Garcia et al., 2019; Griffiths et al., 2017). Lake ice interacts with the under-ice water body to further drive or facilitate the migration and transformation of nutrients and metals, resulting in changes in the phytoplankton biomass (Cavaliere and Baulch, 2018; Schroth et al., 2015). In addition, the ecosystem under the ice affects the limnology of the following seasons (Hampton et al., 2017). pH, electrical conductivity, and chlorophyll *a* are important indicators of the ecological environment and have significant impacts on the primary production, but it is uncommon to see field data of them in the ice decay period. In general, the lack of knowledge of the role of ice melting in ecological and biogeochemical processes limits the proper assessment of the impact of climate change on cold region lakes (Tan et al., 2018).

Due to the difficult fieldwork conditions on deteriorating ice cover, there has not been much in situ research during the ice decay period. A snow cover delays the melting by its high albedo and low transmissivity of light (Ashton, 1986; Leppäranta, 2015; Warren, 1982). When the ice cover is snow-free, sunlight penetrates to the ice and through the ice. The ice warms up and melts inside, the under-ice water is heated, and the surface heat balance determines whether surface melting takes place (Kirillin et al., 2012). Ice impurities are released from melting ice into the water that changes the water environment. The under-ice light is also used for primary production, which normally peaks after ice breakup.

The present knowledge of the melting rate of ice is limited to a few studies, showing typical values of 1–3 cm d^{-1} in terms of equivalent ice thickness. Melting takes place at the top and bottom boundaries and in the interior depending on the weather conditions (Jakkila et al., 2009; Leppäranta et al., 2010, 2019; Wang et al., 2005). It has been found that the light transmittance changes with internal melting that has influence on further melting. Internal melting also opens channels for flushing the ice by surface meltwater and lake water. When the porosity of ice reaches the level of around 0.5, the ice cover collapses by its own weight and disappears rapidly (Leppäranta et al., 2010, 2019). Bottom melting is

82 caused by the heat flux from water that can be large in spring due to the solar heating of the under-ice
83 water (Jakkila et al., 2009; Shirasawa et al., 2006).

84 We examine here the decay of ice in a boreal lake, Lake Pääjärvi, in southern Finland by field
85 surveys in two years, 2018 and 2022. The objective was to analyse the ice melting process for the
86 evolution of ice thickness and porosity as well as for the changes in ice and water geochemistry. The
87 structure and properties of ice experienced remarkable changes during the decay process, and
88 significant melting occurred in the surface and bottom and in the interior. Flushing of ice by meltwater
89 and lake water caused changes to ice and water geochemistry. A deeper knowledge of the ice decay is
90 needed for modelling the lake ice decay, particularly for ice engineering issues, and for understanding
91 the physical and geochemical conditions for ecology of freezing lakes in spring. This paper gives the
92 results of the Lake Pääjärvi field program.

93 **2 Materials and methods**

94 **2.1 Study site**

95 Lake Pääjärvi is located in the boreal zone in southern Finland (61°40′ N, 25°08′ E). The lake area is
96 13.4 km^2, the mean and maximum depths are 14.4 m and 87 m, respectively, and the catchment area is
97 244 km^2 (Arvola et al., 1996). Lake Pääjärvi is a humic, brown-water lake with an average optical depth
98 of 0.67 m and Secchi depth of 1.8 m (Arst et al., 2008). The decay of the ice cover takes about one
99 month, controlled by the presence of snow on top, the optical quality of snow and ice, and the
100 atmospheric and solar forcing (Wang et al., 2005; Jakkila et al., 2009). The LBS ice phenology data
101 base shows that in 1970–2022 the ice breakup date was on average April 25, with a standard deviation
102 of 12 days. In 1993–1999, the maximum annual ice thickness was on average 46 cm with the standard
103 deviation of 12 cm, and the fraction of snow-ice was on average one-third (Leppäranta and Kosloff,
104 2000).

105 The field study was made in Pappilanlahti Bay in the west side of the lake near the Lammi
106 Biological Station (LBS). The bay is shallow (maximum depth 12 m), with three small inflow brooks
107 and a weak groundwater flux at the bottom. The field site was about 100 m from the shore with access

first by foot and in late season by a hydrocopter and a boat. Our field program included a pilot study in 12–20 April 2018 and the main experiment in 25 March – 3 May 2022, which was more extensive and provided the main body of the data. The ice situation was recorded by ground photographs, drone orthophotos, and field notes, and ice and water samples were collected at regular field visits. In 2022 the whole decay period was mapped while in 2018 just the last eight days of it.

2.2 Observations

In the pilot study in 2018, the field site was visited five times between April 12 and April 20. The study was focused on a short period at the end of the ice decay. Ice samples were taken on April 12, 15 and 20, and thereafter, because of the rapid melting, it was not possible to walk on the ice or to use a boat for sampling, but photographs were taken daily from the shore. Analyses of samples were made in similar manner as in the main experiment (see below).

The study period in 2022 covered the whole decay period from March 25 to May 3 with eight field site visits. The sampling was made by foot from the shore until April 22. Then an open water zone formed at the shoreline, and a hydrocopter was used for ice sampling on April 26–29 (Fig. 1a). On May 3, the melting created several open channels, and a boat was used for the sampling. Each time the quality and thickness of ice were recorded first with the freeboard, snow thickness, snow-ice thickness, and congelation ice thickness measured by a ruler. Ice samples (cross-section 30 cm × 30 cm) were cut by drill and saw, put in plastic bags, and transported immediately to a freezer (temperature –18 °C) in LBS. Water samples were taken from the drill holes and stored in sealed bottles in a fridge at a temperature of 4–6 °C.

(a) (b)
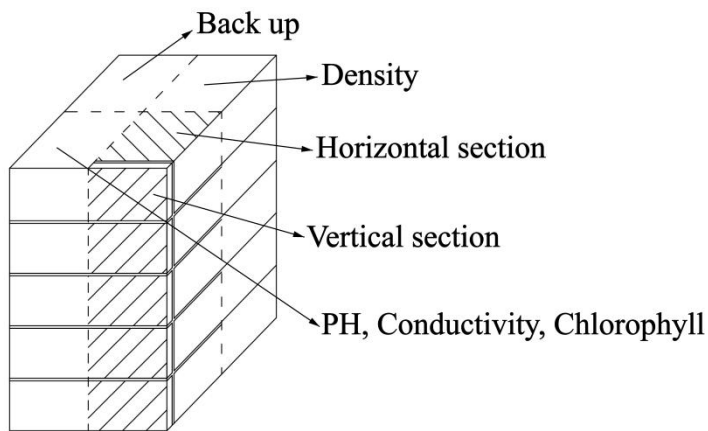
Figure 1. Lake ice sampling and processing: (a) collect ice with a handsaw on the hydrocopter; (b) the ice block was sliced into four parts for different observations.

Available routine meteorological and hydrological data of the Finnish Meteorological Institute (FMI) and Finnish Environment Institute (SYKE) were utilized. The SYKE data include manual measurements of the thicknesses of ice, snow-ice and snow, and freeboard every ten days during the whole winter in Pappilanlahti Bay, and they were used for the all-season ice and snow thickness reference and control. FMI provided the meteorological data of an automated station in LBS yard half a kilometre from our lake site and solar radiation data for the closest radiation site in Jokioinen. The LBS data base was utilized for the long-term ice phenology and geochemistry of the lake and inflow brooks of the study bay.

2.3 Laboratory work

The ice samples were analysed in the INAR (Institute of Atmospheric and Earth Sciences, University of Helsinki) ice laboratory (-10 °C). Each ice sample was divided into four sections. Section 1 was cut vertically into layers for the geochemistry analyses from meltwater in the water laboratory. Section 2 was cut vertically and horizontally to map the ice crystal structure and study the gas bubbles by image analysis, and Section 3 was cut vertically to layers to measure the density of ice. Section 4 was stored as a backup (Fig. 1b).

The samples were cut into vertical sections of $8 - 10$ cm height by a bandsaw, and horizontal sections were extracted at the vertical cuts. The size and distribution of gas bubbles in the ice were

observed under normal light (Deng et al., 2019). The sections were frozen on glass plates to be prepared for thin sections, and the crystal structure of ice was obtained from the thin sections between crossed polarizers (Langway, 1958). The mass/volume method was used to measure the ice density in the laboratory, and the freeboard in the field was used as a control. The sample was cut into 5 cm cuboids by a bandsaw. The sides of a cuboid were measured by a vernier caliper, and the mass was measured by an electronic scale with the accuracy of 0.001 g. The accuracy of the density is estimated as 10 kg m^{-3} determined by the accuracy of the volume measurement.

The water samples as well as the ice meltwater samples were analysed in the LBS water laboratory for pH, electrical conductivity (EC) and chlorophyll *a* (Chl *a*). The ice geochemistry samples were first cut in the ice laboratory into vertical sections based on the structure at intervals of 8 – 10 cm by a bandsaw, melted in sealed bags, poured into sample bottles, and stored in a fridge (at 4–6 ℃). pH and EC were measured from unfiltered samples according to the standards in SFS-EN 27888 and SFS 3021 using a Thermo Orion 3-STAR Precision Benchtop pH meter (accuracy 0.01) and YSI 3200 conductivity sensor (accuracy 0.01 μS cm^{-1}). The Chl *a* concentration was measured from the light absorbance at 665 and 750 nm wavelengths (Arvola et al. 2014).

3 Results

3.1 Ice structure

3.1.1 Ice structure in the pilot study 2018

In 2018, the ice decay period began at the end of March, and the final breakup took place on April 25. The thickness of ice was 42 cm on March 30, and on April 12 it was 35 cm with 5.3 cm snow-ice and 29.7 cm congelation ice (Table 1). Snow-ice melted in less than eight days, and congelation ice melted fast after April 15. On April 24, rain greatly accelerated the melting.

Table 1. Thickness of ice layers and freeboard in the melting phase (cm) and porosity (%) in April 2018, also shown is the ratio of freeboard (Fb) to draft.

2018	Snow-ice	Congelation ice	Total ice	Porosity	Freeboard	Fb/draft
April 12	5.3	29.7	35.0	~ 0	3.0	0.094
April 13	4.7	29.3	34.0	x	3.0	0.097
April 14	3.3	28.7	32.0	x	2.0	0.067

April 15	2.7	28.3	31.0	x	2.0	0.069
April 20	0	20.3	20.3	25	x	x
April 25	0	0	0	x	0	x

3.1.2 Ice structure in the main experiment 2022

The ice decay period began on March 25 and the final breakup took place after 42 days on May 5 (Table 2). The thickness of ice was 55 cm on March 25, close to the long-term mean, with 33 cm congelation ice and 22 cm snow-ice. During the decay period the ice was melting at both boundaries and in the interior. At the end of April there was a slush layer between the surface ice layer and the congelation ice layer with soft places so that walking on the ice was not easy.

Table 2. Thickness of ice layers and freeboard in the melting phase (cm) and porosity (%) in 2022, also shown is the ratio of freeboard (Fb) to draft. x stands for no data.

2022	Snow-ice	Congelation ice	Total ice	Porosity	Freeboard	Fb/draft	Snow
March 25	33	22	55	x	5.5	0.11	1
April 1	31	20	51	6.1	5	0.11	2.5
April 8	30	17	47	x	2	0.044	13
April 14	31	17	48	7.7	5	0.12	2
April 22	27	11	38	15.2	4	0.12	0
April 26	7.5 + 7¶	10	24.5	17.1	1	0.043	0
April 29	6 + 12¶	4	22	24.1	0.5	0.023	0
May 3	2	0	2	34.0	x	x	0
May 5	0	0	0	x	0	x	0

¶ Surface ice + slush layer

Figure 2 shows drone orthophotos of the ice cover taken at an altitude of 100 m during the melting period. As reported by Ashton (1985) about melting lake ice in general, the ice cover of Lake Pääjärvi looked grayish and patchy from above. Snowfall turned the ice white at the beginning of April, and as the air temperature increased, the new snow began to melt creating a patchy surface. The positive albedo feedback of melting ice supports the persistence of surface patchiness.
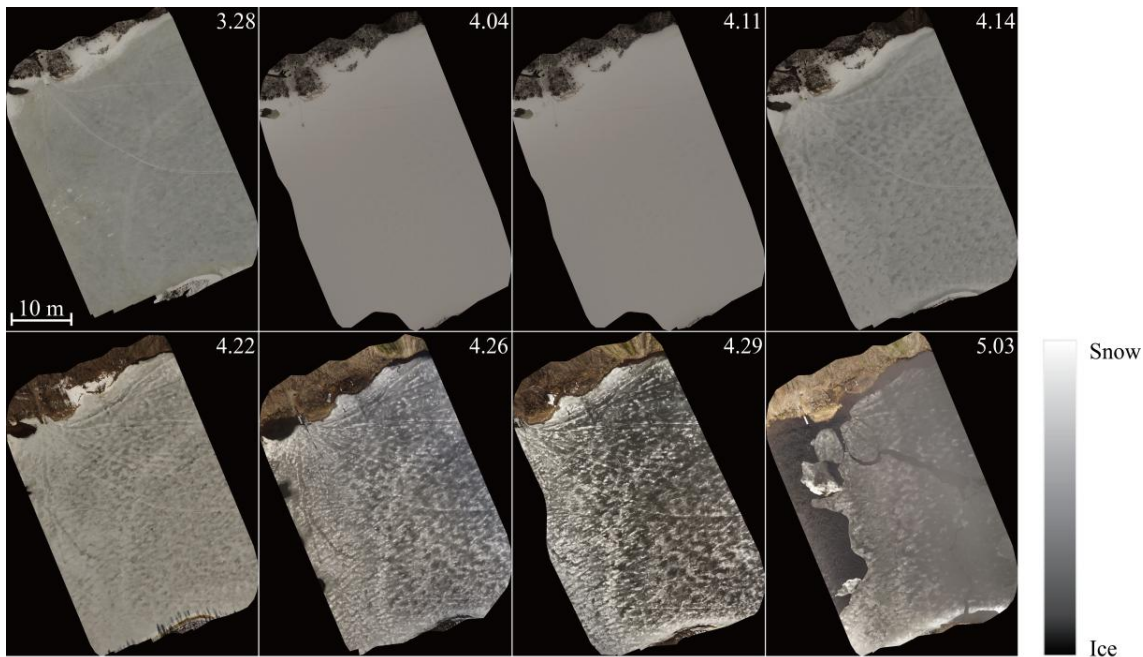
186

187 **Figure 2.** Drone orthophotos of the ice cover in the melting period in 2022 (time given as month.day).

188   There were two principle vertical layers in the Lake Pääjärvi ice cover (Fig. 3). The top layer was
189 granular snow-ice, with the grain size of $1-9$ mm and blurred crystal boundaries, and the lower layer
190 was clear columnar congelation ice with the grain size of $2-10$ cm. When the ice melting progressed,
191 the ice crystal structure data showed that the thickness of both snow-ice and congelation ice decreased,
192 and the porosity of ice increased.

193   The ice melted 4 cm in May 25–April 1. On April 1, the snow-ice part had two sub-layers (Fig. 3).
194 The top 27 cm sub-layer had very irregular crystal structure with blurred crystal boundaries and grain
195 size mainly within $1-2$ mm. In the lower, $27-31$ cm, layer the crystals were granular with clear
196 boundaries, and the grain size was mainly $2-5$ mm. It was judged that the upper sub-layer had
197 undergone thawing and refreezing process. The columnar ice layer underneath was clear ice with grain
198 size increasing with depth, from 2 to 10 cm. The volume fraction of gas bubbles was $4-6$ % in the
199 snow-ice layer. They were cylindrical and spherical shaped with the maximum diameter of 4 mm. The
200 corresponding fraction was $1-2$ % in congelation ice, the bubbles were spherical with the maximum
201 diameter of 1 mm.

In April 1–14 congelation ice melted by 3 cm, but snow-ice thickness was unchanged. According to the weather data, a snowfall began on April 5, and then the air temperature rose resulting in the formation of new snow-ice through the melt–freeze cycle. Compared with April 1, the ice crystal size had not changed, and the gas volume of snow-ice was 5–7 %. After April 14, the air temperature increased further, and the ice melted by 10 cm in April 14–22. The horizontal and vertical sections showed strong melting at the grain boundaries in snow-ice (Fig. 4a). The gas content increased in snow-ice to 6–10 % and in congelation ice to 1–3 %. Also, the maximum diameter of gas bubbles increased to 5 mm in snow-ice and 3 mm in congelation ice.

In April 26–29, a slush layer appeared below a surface ice layer due to internal melting of ice (Fig. 4b). The columnar ice began to melt at crystal boundaries where gas inclusions appeared. On April 29, the gas volume reached 5 % in the columnar layer, with the maximum bubble size equal to 5 mm. On May 3, the columnar ice and slush layers had melted, and there was only 2 cm snow-ice left (Fig. 4c).
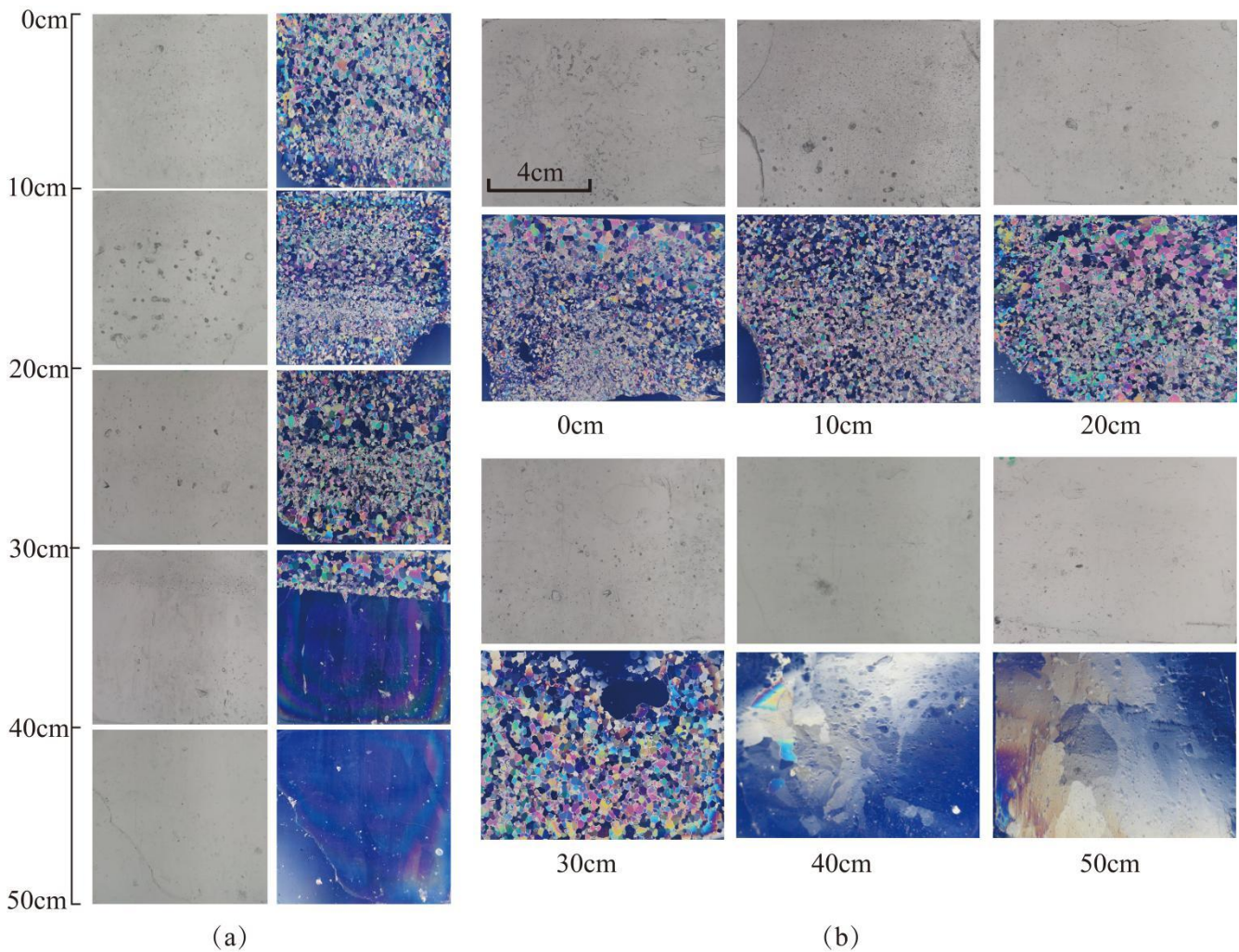
Figure 3. Lake Pääjärvi ice crystal structure of April 1. (a) vertical profiles under the normal light (left) and ice crystal structure under the polarized light (right), (b) horizontal sections under the normal light (top) and ice crystal structure under the polarized light (bottom).

218 (a) (b) (c)
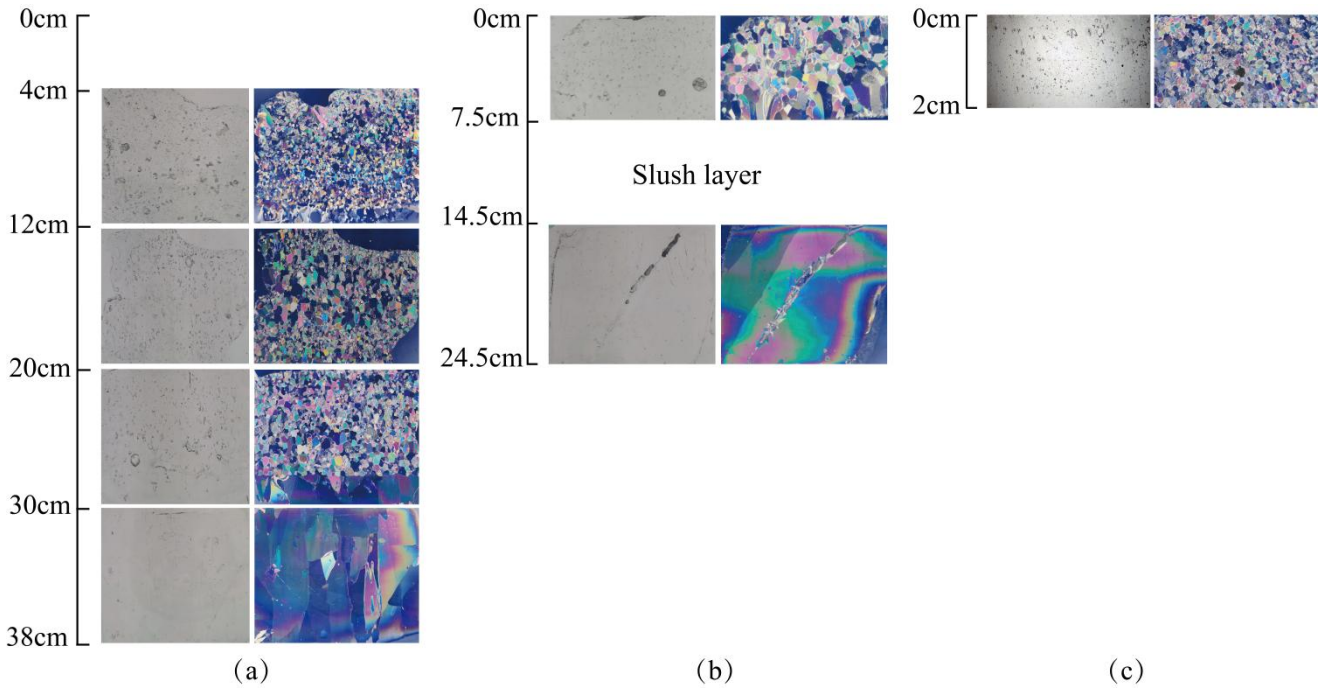
219 **Figure 4.** Lake Pääjärvi ice crystal structure of April 22, April 26, and May 3. (a) vertical profiles under the
220 normal light (left) and ice crystal structure under the polarized light (right) on April 22; (b) vertical profiles
221 under the normal light (left) and ice crystal structure under the polarized light (right) on April 26; (c) vertical
222 profiles under the normal light (left) and ice crystal structure under the polarized light (right) on May 3.

3.1.3 Ice melt rate

224   The ice sample data in Tables 1–2 were used to estimate the melting at the surface and bottom and
225 in the ice interior. The melting rate increased toward the breakup date. In 2018 the ice cover was
226 different from 2022 in that the ice was mostly (85 %) congelation ice (Table 1). In April 12–20 the
227 mean surface and bottom melting together was 1.84 cm d^{-1}, and the mean internal melting was 0.86 cm
228 d^{-1}. In April 12–15 the mean surface and bottom melting were 0.87 cm d^{-1} and 0.47 cm d^{-1}, respectively.
229 The ice was more transparent than in 2022 that allowed more sunlight penetration through ice. The
230 bottom melting in 12–15 April corresponded to the heat flux

$$Q = \frac{\rho_i L_f \Delta h}{\Delta t} = 16 \text{ W m}^{-2} \tag{1}$$

232 where ρ_i is ice density, L_f is the latent heat of freezing, Δh is the change in ice thickness, and $\Delta t =$
233 1 d.

Table 3. Ice melting in spring 2018 (cm). The numbers show the change from the row above to the present one. At the end, surface melting and bottom melting cannot be separated from the data as shown by z_1 and z_2. x is for no data.

2018	Surface melt	Bottom melt	Total melt	Internal melt
April 12	0	0	0	0
April 13	0.6	0.4	1.0	x
April 14	1.4	0.6	2.0	x
April 15	0.6	0.4	1.0	x
April 20	2.7+ z_1	8.0 – z_1	10.7	6.9
April 25	z_2	20.3–z_2	20.3	x

In 2022 the mean rate was 1.31 cm d^{-1}, and snow-ice melted a little faster than congelation ice. The mean melt rates were, respectively, 0.79 cm d^{-1} and 0.38 cm d^{-1}. There was a minor new snow-ice formation on April 14, and the last 2 cm thick piece was snow-ice on May 3. The mean melt rate at the bottom corresponds to the heat flux of 13 W m^{-2} from water to ice. This flux was larger than normally assumed (e.g., Yang et al., 2012). The mean internal melt rate was 0.18 cm d^{-1} equivalent ice thickness that was smaller than the surface and bottom melting, attributed to the low light transmittance of snow-ice. In the last week of melting, the ice was highly porous and internal breakages occurred.

Table 4. Ice melting in spring 2022 (cm). The numbers show the change from the row above to the present one.

2022	Surface melt	Bottom melt	Total melt	Internal melt
March 25	0	0	0	0
April 1	2	2	4	x
April 8	1	3	4	0.4
April 14	-1	0	-1	0.4
April 22	4	6	10	3.2
April 26	4.5	1	5.5	0.6
April 29	4.5	6	10.5	1.6
May 3	16	4	20	1.2
May 5	2	0	2	0
Sum	33	22	55	7.4

3.2 Ice density

At the initial stage of melting, April 1 – 14, 2022, the estimated average densities of snow-ice and congelation ice were 850 kg m^{-3} and 930 kg m^{-3}, respectively. The congelation ice data are from the deep layers, and the apparently high density is likely due to liquid water in pores. The density profiles shifted toward lower level with time while the density always increased with depth (Fig. 5). On April 22

250   the snow-ice density was higher than on April 14 at large depth that can be due to meltwater

251   accumulation in deep pores. Toward the ice breakup, the density decreased, in snow-ice to below 700

252   kg m^{-3} and in congelation ice to almost 700 kg m^{-3}. The density data were used to estimate the porosity,

253   which was found to increase from 6.1 % to 34 % during the melting period (Table 2).
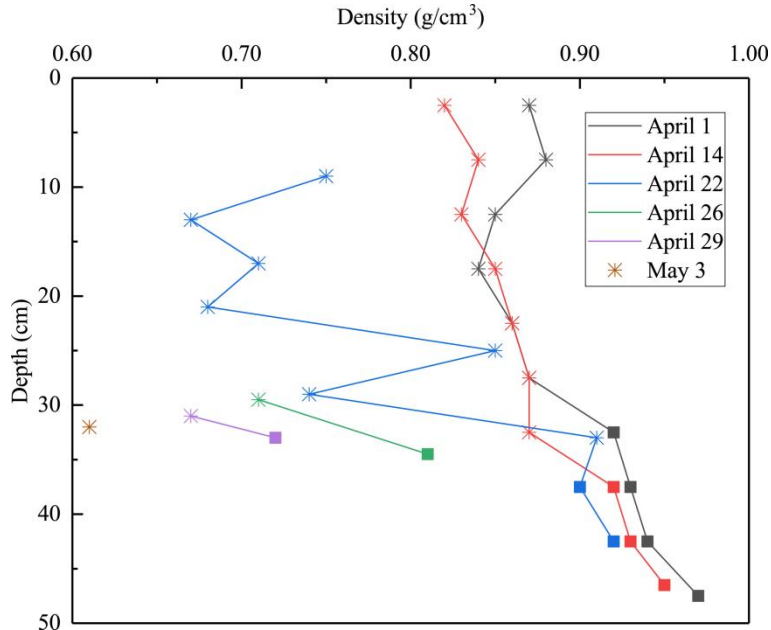
254

255   **Figure 5.** Lake Pääjärvi ice density profiles in 2022 (asterisk stands for snow-ice, square for congelation ice).

256   For bare ice, the freeboard/draft ratio is

$$\frac{h_f}{h_d} = \frac{\rho_w - \rho_d}{\rho_f} \tag{2}$$

257

258   where h is thickness and ρ is density, and the subscripts are w for water, d for draft, and f for

259   freeboard. In winter, for $\rho_f \approx \rho_d \approx 910$ kg m^{-3}, this ratio is 0.10. It increases when the porosity

260   decreases evenly, but it decreases if meltwater drainage from freeboard is trapped inside the draft to

261   reduce the buoyancy. This is consistent with the present field observations.

262   **3.3 Heat budget**

263   We consider the volume of ice per unit area (V), expressed by the ice thickness (h) and porosity (v)

264   as $V = (1 - v)h$. The external heat fluxes include the surface flux Q_0, the heat flux from water to ice

bottom Q_w, and the absorption of solar radiation inside ice Q_A. It is assumed that in the melting stage the ice is isothermal with the temperature at the melting point. The heat fluxes are taken positive toward the ice, and for simplicity negative fluxes are ignored, i.e., the model heat flux is $Q_0^+ = \max(Q_0, 0)$. The surface and bottom fluxes reduce the thickness of ice, while the internal heating increases the porosity. Thus, we have (Leppäranta et al., 2019)

$$\rho_i L_f (1 - v) \frac{dh}{dt} = -(Q_0^+ + Q_w) \tag{3a}$$

$$\rho_i L_f h \frac{dv}{dt} = Q_A \tag{3b}$$

At $v = v^* \sim 1/2$, the ice breaks due to its own weight and the remaining ice pieces melt fast.

Here the surface heat flux is based on air temperature due to the lack of more complete atmospheric observations. The linearized approximate formula of Leppäranta (2015) is employed:

$$Q_0 = k_0(t) + k_1(T_a - T_0) \tag{4}$$

where k_0 is independent of the surface temperature but depends on time, and $k_1 \sim 15$ W m^{-2} °C^{-1}. In exact terms, k_0 includes the radiation balance and latent heat flux at $T_a = T_0$, and their correction for $T_a \neq T_0$ plus the sensible heat flux is included in k_1. In Lake Pääjärvi, k_0 varies between -50 W m^{-2} and 115 W m^{-2} in summer (Leppäranta and Wen, 2022). The second term in Eq. (4) represents the common degree-day model of ice melting, while the first term is geographic representing the location (Leppäranta and Wen, 2022). The given value of k_1 corresponds to the degree-day coefficient of 0.43 cm (°C·d)$^{-1}$, which is close to the usual degree-day coefficient in hydrological forecasting (Leppäranta, 2015).

The internal melting and bottom melting depend on the solar radiation. We have (see Leppäranta et al., 2019)

$$Q_A = (1 - \alpha)\gamma(1 - e^{-\lambda h})Q_{s0} \tag{5}$$

$$Q_w = Q_{w0} + c(1 - \alpha)\gamma e^{-\lambda h}Q_{s0} \tag{6}$$

where α is albedo, $\gamma \approx 0.5$ represents the fraction of solar radiation that penetrates the surface (the light band), λ is the light attenuation coefficient, and c is the fraction of under-ice solar heating

returning to ice bottom. Eq. (5) gives the part of solar radiation used for internal melting, and the bottom melting in Eq. (6) consists of the background heat flux from the deep water (Q_{w0}) and a part of the under-ice solar radiation.

The heat fluxes for ice melting in 2022 were estimated from Eqs. (4-6). The forcing was provided by the solar radiation data of FMI station Jokioinen and by the air temperature data of FMI station Lammi. It was assumed that the surface temperature was at the melting point. The incident solar radiation averaged to 126 W m^{-2} in the last week of March and 198 W m^{-2} in the first week of May, and the maximum daily average was 268 W m^{-2}, on April 25. The albedo was parameterized as $\alpha = 0.7$ for snow, 0.5 for dry ice and 0.3 for wet ice, and $\lambda = 0.5$ m^{-1} was fixed. The mean solar radiation and the mean air temperature were 184 W m^{-2} and 2.4 °C in April 2022, while the corresponding climatological values are 152 W m^{-2} and 3.5 °C.

The function k_0 was estimated based on Leppäranta (2015): k_0 increased from -35 W m^{-2} on March 25 to -1 W m^{-2} on May 5. The total modelled surface melting became 36.6 cm, which is rather close to the observation (33 cm) obtained from the ice structure analysis (Table 3). The resulting mean absorption of solar radiation by ice was $Q_A = 5.6$ W m^{-2} corresponding to the melt rate of 0.16 cm d^{-1}, close to 0.18 cm d^{-1} obtained from the ice structure data. To evaluate the heat flux from the water, we took $c = 0.3$ (Leppäranta et al., 2019), and then the contribution of solar radiation to the heat flux to ice bottom became 10.5 W m^{-2}. The background term Q_{w0} is not known but for molecular conduction the scale is $Q_{w0} = k_w \, \partial T / \partial z \sim 1$ W m^{-2}, where $k_w = 0.56$ W m^{-1} °C^{-1} is thermal conductivity of water, and in general mid-winter data suggest that $Q_{w0} < 5$ W m^{-2}. With $Q_{w0} = 1$ W m^{-2}, we have $Q_w = 11.5$ W m^{-2} and the corresponding melt rate at the ice bottom would be 0.33 cm d^{-1}. This result is supported by the estimate $Q_w = 13$ W m^{-2} from the ice structure data in Section 3.1.

Ice melting obtained from the ice structure data is illustrated in Fig. 6. In 2022, the surface melting was greater than the bottom melting, while in 2018, it was the opposite. The main reason for this difference was in the ice stratification. In 2022, the snow-ice layer accounted for 60 % of the ice cover, while in 2018, the fraction was only 15 %. The melting rate was gradually increasing with the weather getting warmer and solar radiation increasing with time.
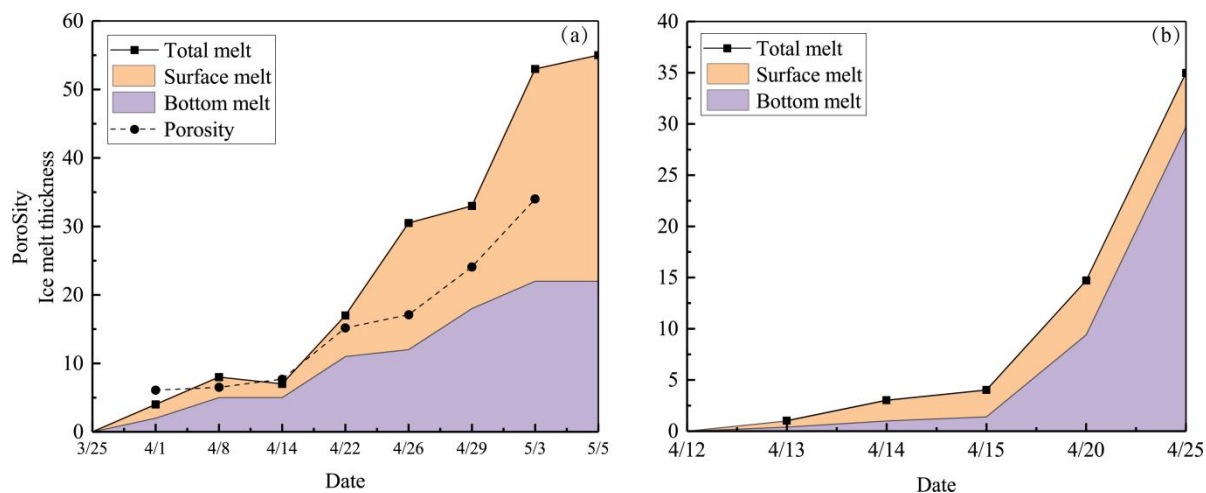
317

318 **Figure 6.** Accumulated ice melting and porosity in 2022 (left) and 2018 (right) based on field data of ice
319 structure. Porosity was not recorded in 2018.

320 **3.4 Ice geochemistry**

321 During the ice decay period, meltwater was mixed into the under-ice water layer that influenced the
322 water geochemistry. In the present data the meltwater had lower pH and EC than the lake water (Figs.
323 7–8). On April 1, 2022, the mean pH and EC of snow-ice were 6.38 and 17.3 μS cm^{-1}, respectively, and
324 in congelation ice the corresponding values were 6.75 and 9.0 μS cm^{-1}. Atmospheric deposition of
325 acidic substances was judged as the background for the low pH of snow-ice. Then pH and EC decreased.
326 The vertical profiles of EC, pH and Chl a show that EC was larger near the snow-ice surface than in
327 congelation ice in the early melting stage, but the difference was no more obvious after April 14. pH
328 was always smaller in snow-ice than in congelation ice. Chl a content was less than 0.6 μg L^{-1} with the
329 maximum at the snow-ice–congelation ice interface. In 2018, the limited data showed that EC was 6 μS
330 cm^{-1} and pH was 6.35 in ice.

331 In lake water, the mean $\pm$ standard deviation of pH and EC were 6.82 $\pm$ 0.09 and 92.5 $\pm$ 12.7 μS
332 cm^{-1}, respectively, in 2022. EC was smaller in ice by one order of magnitude than in water, on average
333 EC(ice) = 0.12·EC(water). EC was decreasing with time in water due to meltwater drainage from ice
334 (Fig. 8). The changes in pH and EC had both signs, caused by flushing by meltwater and lake water. pH
335 increased in the late melting period after the slush layer appeared, likely due to the increase in the

336 photosynthesis enhanced CO_2 consumption. However, the inflow from brooks into the study bay could
337 cause an opposite effect (Fig. 9). The inflow was weak until April 21, but in April 21–25 it
338 corresponded to 17 % of the water volume of the bay.

339
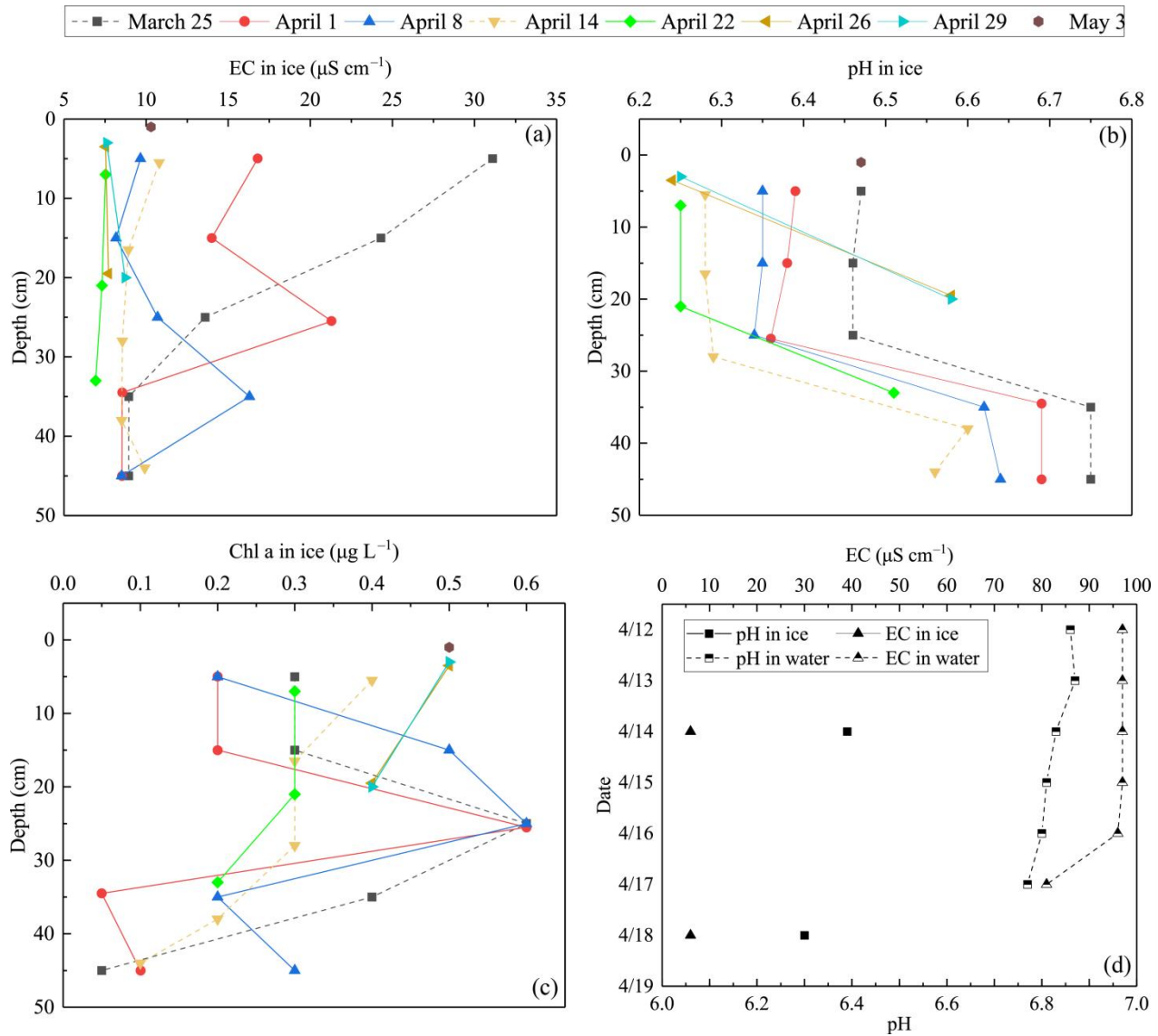
Figure 7. EC, pH and Chl *a* in ice meltwater and under-ice water at the study site in 2022 and 2018. (a) EC in ice meltwater and under-ice water at the study site in 2022; (b) pH in ice meltwater and under-ice water at the study site in 2022; (c) Chl *a* in ice meltwater and under-ice water at the study site in 2022; (d) EC and pH in ice meltwater and under-ice water at the study site in 2018.

344
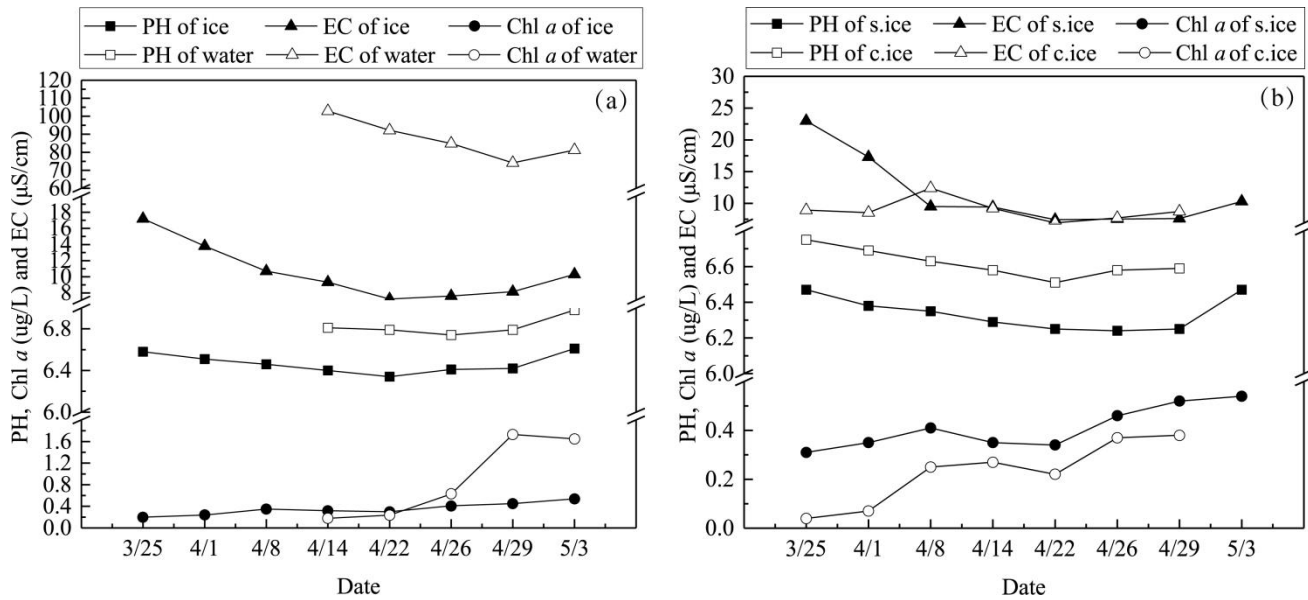
Figure 8. The mean pH, EC and Chl *a* in ice and lake water in 2022 (left) and the mean pH, EC and Chl *a* in
346 snow-ice (s.ice) and congelation ice (c.ice) (right).

347   Algae can grow under ice and in slush layers in ice all winter at sufficient photon flux conditions.
348 In springtime algae growth occurs also in pores in ice containing liquid water. Chl *a* content was similar
349 in under-ice water and in ice until April 26, but then it increased in water and became much higher than
350 in ice at the time of ice breakup, but still well below the first summer peak.

351
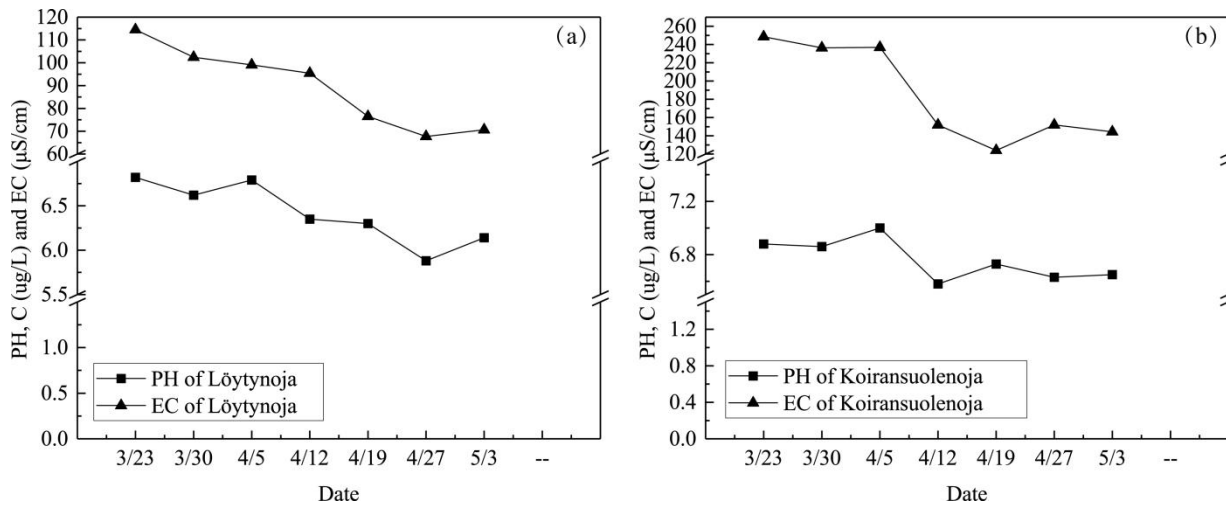
Figure 9. pH and EC in two inflow brooks, Löytynoja (left) and Koiransuolenoja (right), to the Pappilanlahti
353 Bay.

4 Discussion

4.1 Interannual variations of ice breakup date

Field data of lake ice are very important to examine and predict ice phenology and the ice break up date is an significant ice phenological parameter during ice melting period (George, 2007; Williams et al., 2004; Stefen and Fang 1997). Based on the ice break data from the Lammi Biological Station, we can see the interannual variations of ice breakup date in a boreal lake, Pääjärvi. The date of ice breakup is largely affected by solar radiation and the thickness and structure of ice and snow layers. Snow cover blocks the atmospheric and solar heat fluxes to the ice and prevents deterioration of the ice under snow. The first critical time in ice decay is the snow melting. Due to the positive albedo feedback and increasing solar radiation, it is difficult to pause melting. The melt rate of ice is $1-3$ cm d^{-1}, increasing with time.

The ice breakup date has become earlier in the last 50 years in Lake Pääjärvi, but the interannual variability has been large (Fig. 10). In 1970–1990 the change was about 5 days per decade that is more than can be explained by the regional warming, and the reason remains unclear. In general, in southern Finland the trend of the breakup date is $0.5-1$ day earlier per decade as is typical in the global scale (Bernhardt et al., 2011; Magnuson et al., 2000). In northern Finland, Lake Kilpisjärvi, the trend from 1964 to 2008 was 0.44 days over a decade towards earlier ice breakup (Lei et al., 2012). Earlier ice breakup has a potentially widespread implications on 50 countries (Sharma et al., 2019). The loss of lake ice may lead to a reduction in the availability of fresh water due to increased evaporation, as well as to cultural and socio-economic impacts to lake ice recreation, such as ice fishing and skating.
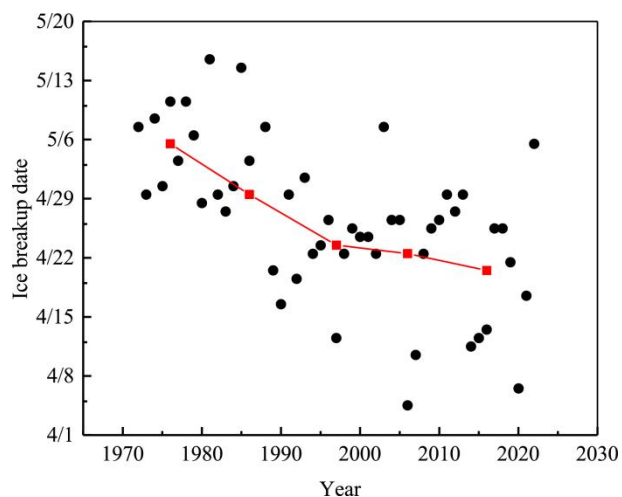
374

375 **Figure 10.** The ice breakup date of Lake Pääjärvi in 1970–2022. The black dots show the breakup date and the
376 red squares show the ice breakup date averaged in every 10 years. Data source: Lammi Biological Station.

4.2 Comparisons of ice melting with other lakes

378 Melting of ice begins when the heat balance turns positive in spring and takes place at the surface,
379 interior and bottom depending on the ice structure and fluxes. In 2022, the mean melting rate was 0.79
380 cm d^{-1} at the surface, 0.52 cm d^{-1} at the bottom, and 0.18 cm d^{-1} in the ice interior in Lake Pääjärvi. In
381 an Arctic tundra lake in northern Finland, Lake Kilpisjärvi, the triple (surface, bottom, and internal
382 melting) was (2.9, 0.5, 1.0) cm d^{-1} in a warm spring 2013 and (0.8, 0.1, 1.0) cm d^{-1} in a normal spring
383 2014 (Leppäranta et al., 2019). In a boreal lake, Lake Vendyurskoe, at 61–62°N, field investigations in
384 two seasons showed the mean melt rates of 1.2 cm d^{-1} at the surface in both cases and 0.8 and 0.2 cm
385 d^{-1} at the bottom (Leppäranta et al., 2010). The differences in the quality of melting are due to
386 differences in the congelation ice/snow-ice fractions and weather conditions that determine the level of
387 light transfer through ice and surface heat balance.

388   The porosity of ice needs to be estimated to examine the internal melting process. In the present
389 work, the porosity was estimated from the measured ice density directly and from the absorbed solar
390 radiation indirectly. The results were consistent with each other. Increasing porosity during the melting
391 period changes the ice structure and decreases the strength of ice, and finally leads to breakage with
392 rapid final disappearance of ice. Here the breakage took place in May 3–5 when the porosity of the ice

was $40-50$ %. Leppäranta et al. (2019) used the solar radiation method to evaluate the porosity and found the same level at the breakage supporting our result.

The heat flux from the lake water body to the bottom of ice has not been much studied (Shirasawa et al., 2006; Kirillin et al., 2012). A heat flux of the order of 1 W m^{-2} represents molecular conduction in the near-surface water layer and may be feasible in mid-winter (e.g., Jakkila et al., 2009; Kirillin et al., 2012; Yang et al., 2012), but in spring, penetration of solar radiation to the water body gives a fractional return flux to the ice bottom. According to the present study, the heat flux from water to ice scales as 10 W m^{-2} in melting period, and the more transparent ice allowed more sunlight penetration and larger heat flux. Jakkila et al. (2009) reported the heat flux values in Lake Pääjärvi as 12 W m^{-2} during the final stage of ice melting that is very close to the present results, while Leppäranta et al. (2019) obtained 15–20 W m^{-2} in a warm spring but less than 5 W m^{-2} in a normal spring in a tundra lake. In the earlier literature, smaller values have been reported even at late stages of ice melting. E.g., Bengtsson et al. (1996) obtained this heat flux ranging within $5-7$ W m^{-2} in March$-$April in small Swedish lakes. Thus the picture of increasing bottom melting is clear, but the question anyway remains the most uncertain component of the heat budget of lake ice, and more research is needed (Kirillin et al., 2018).

The quality of ice decay is important to ice mechanics due to the loss of ice strength (Ashton, 1986; Leppäranta, 2015). There are two important consequences. First, the bearing capacity of ice (P) decreases. This quantity scales as $M \propto \sigma_f h^2$, where σ_f is the flexural strength, and during the melting period ice thickness and strength both decrease, thickness due to melting at the boundaries and strength due to internal melting. The positive albedo feedback in the melting process produces a patchy ice cover, and together with the unpredictable bearing capacity the ice cover becomes a severe safety issue. Secondly, the two-dimensional yield strength of a lake ice cover scales as $P \propto \sigma_c h/L$, where σ_c is the compressive strength of ice and L is the lake size length scale. With decreased thickness and strength, wind stress may lead to ice breakage and ice movement on shores, where damage can be caused to man-made structures since the ice strength is still finite.

4.3 Ice melting impact on geochemistry

Porous melting ice is permeable to water. Meltwater can flow down from top and lake water may penetrate to pores from below that also influences the stratification of the under-ice water layer. Here the basic geochemical properties were studied: pH, EC and Chl a. They provide information about physical and chemical processes. The meltwater has lower EC than the lake water and, consequently, a lower density, and therefore a thin fresh surface layer may form just under the ice (Kirillin et al., 2012). The geochemistry also affects the physiological state of aquatic organisms, which will guide and predict the changes of biological structure in the water during the melting season.

The geochemistry under melting ice has been rarely reported. Lake Pääjärvi was studied for ice and water geochemistry in mid-winter in 1996–1998 (Leppäranta et al., 2003). Their mean EC in ice and water were close to our data, 16.5 and 108 μS cm^{-1}, respectively, as compared with our 9.0 μS cm^{-1} for congelation ice, 17.3 μS cm^{-1} for snow-ice, and 92.5 μS cm^{-1} for water; their mean EC in snow was 13 μS cm^{-1}. In Leppäranta et al. (2003), pH was 6.7 for ice and 6.6 for water, but in our data, pH was a little lower in snow-ice and congelation ice than in lake water. Chl a was less than 0.5 μg L^{-1} in ice and between 0.2 and 1.7 μg L^{-1} in water which is of the same order of magnitude reported by previous research (Leppäranta et al., 2003; Vehmaa and Salonen, 2009). Leppäranta et al. (2003) reported Chl a in ice also less than 0.5 μg L^{-1} in Lake Pääjärvi but about 3 μg L^{-1} in a hypereutrophic lake 100 km from Pääjärvi. The present results are consistent with the previous studies, the small differences can be explained by the differences in the quality of winters.

5 Conclusions

Ice season has a specific role in the local environment and human life, and it has an impact on the lake ecology far beyond the ice period. Research of lake ice has largely increased to evaluate the impact of the predicted climate change on the ice phenology and properties. During the melting period, it is difficult to do fieldwork due to the deterioration of the ice cover, and therefore only few data have been collected. In the present work, ice decay was monitored from the start to the final breakup resulting with a full time-series of the evolution of ice thickness, structure, and geochemical properties.

In 2022, the maximum thickness of ice was 55 cm with 60 % snow-ice, and in 42 days the ice melted by 33 cm from the surface and 22 cm from the bottom while the porosity increased from less than 5 % to 40–50 % at breakup. The comparison between ice structure and heat budget gave a good agreement in quantifying the deterioration of the ice cover. This result is promising when considering the possibility of detailed numerical modelling of ice deterioration. The largest uncertainty is in the bottom melting, where more research is needed on under-ice boundary layer dynamics. Solar radiation penetrating through ice adds a major contribution to the heat flux from water to ice, according to the present results on the order of 10 W m^{-2}, which is significantly higher than usually assumed in lake ice modelling.

Ice and water pH and EC decreased during the ice decay but experienced fluctuations due to flushing by meltwater and lake water. The mean EC of ice was 11.4 μS cm^{-1}, equal to the fraction 0.12 of the lake water EC. The mean ice pH was 6.44, lower by 0.4 than in water. Chl a in ice increased to 0.6 μg L^{-1} in the late part of ice decay, with the maximum in the slush sub-layer of snow ice. At the end of the decay, Chl a was 1.7 μg L^{-1} in water, still far from the first summer maximum.

The results are important for modelling the lake ice season and the annual cycle of lakes. Lake ice has an important role in the physical, chemical, and ecological cycle, and these cycles are sensitive to climate changes. For the ice melting season, detail modelling of the ice strength and the consequent bearing capacity and ice forces has a major importance for the local societies in lake regions.

Data availability. The routine meteorological and hydrological data are available at: https://www.syke.fi and https://www.fmi.fi. The ice samples data applied in this work can be accessed by the link: https://doi.org/10.5281/zenodo.7342770.

Author contributions. YZ conceived the field and laboratory study in 2022 with ML and MF and wrote the paper with contributions from JL and ZL. SS and JA performed the study in 2018. All co-authors discussed the results and edited the manuscript.

Acknowledgements. We are grateful to the Lammi Biological Station and the Institute of Atmospheric and Earth Sciences, University of Helsinki for providing logistical help and laboratories. Thanks to Esa-Pekka Tuominen, Joni Uusitalo and Riitta IIola for helping in the fieldwork and laboratory, and to

Lauri Arvola for comments on the manuscript. This work was financially supported by the National Key Research and Development Program of China (Grant No. 2019YFE0197600), the National Natural Science Foundation of China (Grant No. 52211530038) and the Academy of Finland (350576 and 333889), and a personal grant to Yaodan Zhang by China Scholarship Council (CSC).

Competing interests. The authors declare that they have no conflict of interest.

References

Arst, H., Erm, A., Leppäranta, M., and Reinart, A.: Radiative characteristics of ice-covered freshwater and brackish water bodies, Proc. Estonian Acad. Sci. Geology, 55(1), 3–23, 2006.

Arst, H., Erm, A., Herlevi, A., Kutser, T., Leppäranta, M., Reinart, A., and Virta, J.: Optical properties of boreal lake waters in Finland and Estonia, Boreal Environ. Res., 13, 133–158, 2008.

Arvola, L., Kankaala, P., Tulonen, T., and Ojala, A.: Effects of phosphorus and allochthonous humic matter enrichment on metabolic processes and community structure of plankton in a boreal lake (Lake Pääjärvi), Can. J. Fish. Aquat. Sci., 53, 1646–1662, https://doi.org/10.1139/f96-083, 1996.

Arvola, L., Salonen, K., Keskitalo, J., Tulonen, T., Järvinen, M., and Huotari, J. : Plankton metabolism and sedimentation in a small boreal lake—a long-term perspective, Boreal Environ. Res., 19, 83-96, 2014.

Ashton, G. D.: Deterioration of floating ice covers, J. Energy Resour. Technol.-Trans. ASME, 107, 177–182, https://doi.org/10.1115/1.3231173, 1985.

Ashton, G. D. (Ed.): River and lake ice engineering, Water Resources Publications, Littleton Colorado, 1986.

Benson, B. J., Magnuson, J. J., Jensen, O. P., Card, V. M., Hodgkins, G., Korhonen, J., Livingstone, D. M., Stewart, K. M., Weyhenmeyer, G. A., and Granin N. G.: Extreme events, trends, and variability in Northern Hemisphere lake-ice phenology (1855–2005), Climate Change, 112, 299–323, https://doi.org/10.1007/s10584-011-0212-8, 2012.

Bengtsson, L., and Svensson, T.: Thermal regime of ice covered Swedish lakes, Hydrol. Res., 27, 39–56, 1996.

Bernhardt, J., Engelhardt, C., Kirillin, G., and Matschullat, J.: Lake ice phenology in Berlin–Brandenburg from 1947–2007: observations and model hindcasts, Climatic Change, 112, 791-817, https://doi.org/10.1007/s10584-011-0248-9, 2012.

Cavaliere, E., Baulch, H. M.: Denitrification under lake ice, Biogeochemistry, 137, 285–295, https://doi.org/10.1007/s10533-018-0419-0, 2018.

Deng, Y., Li, Z. K., Li, Z. J., and Wang, J.: The experiment of fracture mechanics characteristics of Yellow River ice, Cold Reg. Sci. Tech., 168, https://doi.org/10.1016/j.coldregions.2019.102896, 2019.

Ellis, A. W., and Johnson, J. J.: Hydroclimatic analysis of snowfall trends associated with the North American Great Lakes, J. Hydrol., 5, 471–486, https://doi.org/10.1175/1525-7541(2004)005<0471:HAOSTA>2.0.CO;2, 2004.

503 Garcia, S. L., Szekely, A. J., Bergvall, C., Schattenhofer, M., and Peura, S.: Decreased snow cover stimulates under-ice
504   primary producers but impairs methanotrophic capacity, mSphere, 4, https://doi.org/10.1128/mSphere.00626-18, 2019.

505 George, G. D.: The impact of the North Atlantic Oscillation on the development of ice on Lake Windermere, Climatic
506   Change 81, 455–468, https://doi.org/10.1007/s10584-006-9115-5, 2007.

507 Griffiths, K., Michelutti, N., Sugar, M., Douglas, M. S. V., and Smol, J. P.: Ice-cover is the principal driver of ecological
508   change in high Arctic lakes and ponds, PLoS One, 12, https://doi.org/10.1371/journal.pone.0172989, 2017.

509 Hampton, S. E., and Galloway, A. W. E., et al.: Ecology under lake ice, Ecol. Lett., 20, 98–111,
510   https://doi.org/10.1111/ele.12699, 2017.

511 Iliescu, D., and Baker, I.: The structure and mechanical properties of river and lake ice, Cold Reg. Sci. Tech., 48, 202–217,
512   https://doi.org/10.1016/j.coldregions.2006.11.002, 2007.

513 Jakkila, J., Leppäranta, M., Kawamura, T., Shirasawa, K., and Salonen K.: Radiation transfer and heat budget during the
514   melting season in Lake Pääjärvi, Aquat. Ecol., 43, 681–692, https://doi.org/10.1007/s10452-009-9275-2, 2009.

515 Karetnikov, S., Leppäranta, M., and Montonen, A.: Time series over 100 years of the ice season in Lake Ladoga, J. Gt.
516   Lakes Res., 43, 979–988, https://doi.org/10.1016/j.jglr.2017.08.010, 2017.

517 Kirillin, G., Leppäranta, M., Terzhevik, A., Granin, N., Bernhardt, J., Engelhardt, C., Efremova, T., Golosov, S., Palshin, N.,
518   Sherstyankin, P., Zdorovennova, G., and Zdorovennov, R.: Physics of seasonally ice-covered lakes: a review, Aquat.
519   Sci., 74, 659–682, https://doi.org/10.1007/s00027-012-0279-y, 2012.

520 Kirillin, G., Aslamov, I., Leppäranta, M., and Lindgren, E.: Turbulent mixing and heat fluxes under lake ice: the role of
521   seiche oscillations, Hydrol. Earth Syst. Sci., 22, 6493-6504, https://doi.org/10.5194/hess-22-6493-2018, 2018.

522 Korhonen, J.: Long-term changes in lake ice cover in Finland, Hydrol. Res., 37, 347–363,
523   https://doi.org/10.2166/nh.2006.019, 2006.

524 Langway, C. C.: Ice fabrics and the universal stage, Department of Defense, Department of the Army, Corps of Engineers,
525   Snow Ice and Permafrost Research Establishment, 1959.

526 Lei, R., Leppäranta, M., Erm, A., Jaatinen, E., and Pärn, O.: Field investigations of apparent optical properties of ice cover in
527   Finnish and Estonian lakes in winter 2009, Est. J. Earth Sci., 60, 50–64, https://doi.org/10.3176/earth.2011.1.05, 2011.

528 Leppäranta, M.: Interpretation of statistics of lake ice time series for climate variability, Hydrol. Res., 45, 673–683,
529   https://doi.org/10.2166/nh.2013.246, 2014.

530 Leppäranta, M.: Freezing of lakes and the evolution of their ice cover, Springer, Berlin-Heidelberg,
531   https://doi.org/10.1007/978-3-642-29081-7, 2015.

532 Leppäranta, M., and Kosloff, P.: The thickness and structure of Lake Pääjärvi ice, Geophysica, 36, 233–248, 2000.

533 Leppäranta, M., and Wen, L. J.: Ice phenology in Eurasian lakes over spatial location and altitude, Water, 14,
534   https://doi.org/10.3390/w14071037, 2022.

535 Leppäranta, M., Tikkanen, M., and Virkanen J.: Observations of ice impurities in some Finnish lakes, Proc. Estonian Acad.
536   Sci. Chem., 52, 59–75, 2003.

537 Leppäranta, M., Terzhevik, A., and Shirasawa, K.: Solar radiation and ice melting in Lake Vendyurskoe, Russian Karelia,
538   Hydrol. Res., 41, 50-62, https://doi.org/10.2166/nh.2010.122, 2010.

539 Leppäranta, M., Lindgren, E., Wen, L. J., and Kirillin, G.: Ice cover decay and heat balance in Lake Kilpisjärvi in Arctic
540   tundra, J. Limnol., 78, 163–175, https://doi.org/10.4081/jlimnol.2019.1879, 2019.

541 Li, Z. J., Jia, Q., Zhang, B. S., Leppäranta, M., Lu, P., Huang, W. F.: Influences of gas bubble and ice density on ice
542   thickness measurement by GPR, Appl. Geophys., 7, 105–113, https://doi.org/10.1007/s11770-010-0234-4, 2010.

543 Magnuson, J., Robertson, D., Benson, B., Wynne, R., Livingstone, D., Arai, T., Assel, R., Barry, R., Card, V., Kuusisto, E.,
544   Granin, N., Prowse, T., Stewart, K., and Vuglinski, V.: Historical trends in lake and river ice cover in the Northern
545   Hemisphere, Science, 289, 1743–1746, https://doi.org/10.1126/science.289.5485.1743, 2000.

546 Masterson D. M.: State of the art of ice bearing capacity and ice construction, Cold Reg. Sci. Tech., 58, 99-112,
547   https://doi.org/10.1016/j.coldregions.2009.04.002, 2009.

548 Rouse, W. R., Binyamin, J., Blanken, P. D., Bussières, N., Duguay C. R., Oswald, C. J., Schertzer, W. M., and Spence, C.:
549   The influence of lakes on the regional energy and water balance of the central Mackenzie River Basin, In: Cold Region
550   Atmospheric and Hydrologic Studies: The Mackenzie GEWEX Experience, edited by Woo, M. K., Springer, Berlin,
551   309–325, 2008a.

552 Rouse, W. R., Blanken, P. D., Duguay, C. R., Oswald, C. J. and Schertzer, W. M. : Climate-lake interactions. In: Cold
553   Region Atmospheric and Hydrologic Studies: The Mackenzie GEWEX Experience, edited by Woo, M. K., Springer,
554   Berlin, 139–160, 2008b.

555 Schroth, A. W., Giles, C. D., Isles, P. D. F., Xu, Y. Y., Perzan, Z., and Druschel, G. K.: Dynamic coupling of iron,
556   manganese, and phosphorus behavior in water and sediment of shallow ice-covered eutrophic lakes, Environ. Sci.
557   Technol., 49, 9758–9767, https://doi.org/10.1021/acs.est.5b02057, 2015.

558 SFS 3008: Determination of total residue and total fixed residue in water, sludge and sediment, Finnish Standards
559   Association (SFS), 1990.

560 SFS-EN 27888: Water quality. Determination of electrical conductivity, Finnish Standards Association (SFS), 1994.

561 Sharma, S., Blagrave, K., Magnuson, J. J., O'Reilly, C. M., Oliver, S.; Batt, R. D., Magee, M. R., Straile, D., Weyhenmeyer,
562   G. A., and Winslow, L.: Widespread loss of lake ice around the Northern Hemisphere in a warming world, Nat. Clim.
563   Chang., 9, 227–231, https://doi.org/10.1038/s41558-018-0393-5, 2019.

564 Shirasawa, K., Leppäranta, M., Kawamura, T., Ishikawa, M., and Takatsuka, T.: Measurements and modelling of the
565   water-ice heat flux in natural waters, Proceedings of the 18th IAHR International Symposium on Ice, Hokkaido
566   University, Sapporo, Japan, 28 August–September 2006, 85–91, 2006.

567 Shoshany, Y., Prialnik, D., Podolak, M.: Monte Carlo modeling of the thermal conductivity of porous cometary ice. Icarus,
568   157, 219–227, https://doi.org/10.1006/icar.2002.6815, 2002.

569 Stefan, H. G., and Fang, X.: Simulated climate change effects on ice and snow covers on lakes in a temperate region, Cold
570   Reg. Sci. Tech., 25, 137–152, https://doi.org/10.1016/S0165-232X(96)00023-7, 1997.

571 Tan, Z., Yao, H. X., and Zhuang, Q. L.: A small temperate lake in the 21st century: Dynamics of water temperature, ice
572   phenology, dissolved oxygen, and chlorophyll a, Water Resour. Res., 54, 4681–4699,
573   https://doi.org/10.1029/2017WR022334, 2018.

574 Vehmaa, A., and Salonen, K.: Development of phytoplankton in Lake Pääjärvi (Finland) during under-ice convective mixing
575   period, Aquat. Ecol., 43, 693–705, https://doi.org/10.1007/s10452-009-9273-4, 2009.

576 Wang, C. X., Shirasawa, K., Leppäranta, M., Ishikawa, M., Huttunen, O., and Takatsuka T.: Solar radiation and ice heat
577   budget during winter 2002–2003 in Lake Pääjärvi, Finland, Verh. Internat. Verein Limnol., 29, 414–417,
578   https://doi.org/10.1080/03680770.2005.11902045, 2005.

579 Warren, S. G.: Optical properties of snow, Rev. Geophys., 20, 67–89, https://doi.org/10.1029/RG020i001p00067, 1982.

580 Williams, G., Layman, K. L. and Stefan, H. G.: Dependence of lake ice covers on climatic, geographic and bathymetric
581   variables, Cold Reg. Sci. Tech., 40, 145–164, https://doi.org/10.1016/j.coldregions.2004.06.010, 2004.

582 Yang, Y., Leppäranta, M., Cheng, B., and Li, Z. J.: Numerical modelling of snow and ice thicknesses in Lake Vanajavesi,
583   Finland, Tellus Ser. A, Dyn. Meteorol. Oceanogr., 64, https://doi.org/10.3402/tellusa.v64i0.17202, 2012.